Crossover Analysis for the Radiometric Calibration of Radar Depth Sounder Data Products

Hara Madhav Talasila

Center for Remote Sensing and Integrated Systems

University of Kansas

Lawrence, USA

hara.madhav@ku.edu

John Paden
Center for Remote Sensing and Integrated Systems
University of Kansas
Lawrence, USA
paden@ku.edu

Abstract—Accurate knowledge of the Earth's melting polar regions is required to develop scientific models to understand and predict ice mass loss and sea-level rise. Data from airborne radar depth sounders have been a valuable asset for polar research groups for decades. Due to the lack of absolute radiometric calibration in many of these datasets, data users only have access to relatively calibrated datasets. System and processing variations over time, whether intentional or not, confound radiometric analysis of the data. Radiometric analysis is important, for example, to the mapping of basal characteristics such as the presence of liquid water and bed type. To solve the calibration problem, we present a data-dependent calibration solution that depends on natural targets that have known radar scattering characteristics (smooth lake and sea surfaces) and crossovers (where flight paths image the same target presenting the opportunity to link the calibration from one flight line to another). Our approach generates a system of linear equations which we can use to estimate the unknown calibration coefficients and use the residuals to provide an error analysis. The crossover analysis uncovered issues with the data products which we address in this work. We also present some interesting waveform properties that are dependent on various crossover parameters such as altitude differences and the angle between the crossing flight paths.

Index Terms—radiometric calibration, crossover analysis, MCoRDS, natural target, radar depth sounder

I. INTRODUCTION

Earth's response to climate change can be observed in irreversible losses to its cryosphere. Scientific reports show an alarmingly increasing trend in metrics such as sea level rise (SLR), ice sheet mass loss, reduction in summer sea ice coverage, frequency of extreme weather events, and risk to coastal geographies [1]. Since 1993, key contributors to SLR are thermal expansion of oceans (42%), melting of temperate glaciers (21%), the Greenland ice sheet (15%), and the Antarctic ice sheet (8%) [2]. Orbital measurements from gravimeters and altimeters show ice mass loss in Greenland (270±21 Gigatons/year) and Antarctica (146±39 Gigatons/year) over the last two decades [3].

Models that predict SLR caused by changes in surface mass balance and dynamic processes in ice sheets highlight the importance and necessity of modeling the uncertainties

This work is funded by the NSF EarthCube award 2126503, Open Polar Radar Software and Service. Center for Remote Sensing and Integrated Systems (CReSIS) was formerly the Center for Remote Sensing and Ice Sheets (CReSIS).

in these projections [4]. Airborne radar data collected over the ice sheets provide wide area coverage of fine-resolution imagery looking at the inside and basal interface of the ice that aids in the understanding of ice dynamics. In particular, it is required to finely map regions around the grounding line (the boundary between grounded and floating ice) [5] because the ice bottom near these lines indicates ice sheet stability [6] that also serves as an important boundary condition for ice flow numerical models [7]. Radar sounding of crevasses, streams, and other subglacial drainage systems helps study calving and crevasse formation [8], [9]. Radar returns have been used to characterize the orientation of ice crystals linked to ice flow, fabric, and viscosity of ice sheets at shallow depths [10]. Detecting the presence of water bodies, type of water bed (frozen or drained) [11], and analyzing subglacial water flow by cross-system calibration [12] highlight the importance of radars in glaciology and also the need for calibration to improve detection and discrimination [13].

Since 1964, the University of Kansas Radar Systems and Remote Sensing Lab has been involved with remote sensing radar development (orbital and airborne) [14]. Established in 2005, CReSIS is a research facility dedicated to advancing radar technologies and models to understand the role of melting ice sheets in SLR. CReSIS hosts more than 1.3 PetaBytes of radar data and has routinely deployed radar sounders since 1993. CReSIS plays a major part in the Open Polar Radar (OPR) initiative along with a few other prominent polar radar groups [15]. Instead of individual fragmented research, the OPR team aims to bring multiple research communities together to produce a standardized, accessible, and opensource polar radar software [16] and data products. The OPR team constitutes nearly 83% of Antarctic radar sounder data and nearly 100% of Greenland and polar sea-ice data [17].

CReSIS currently operates an advanced airborne radar that has been improved over the past 30 years from the original design by Raju Garudachar [18] to the present Multi-channel Coherent Radar Depth Sounder (MCoRDS). Since 1993, various configurations (flight platforms, antennas, transmitter, and receiver architectures) of the depth sounder have flown and collected data from 62 science missions, gathering valuable scientific data about deep layers of ice and bedrock across Greenland, Antarctica, and other polar regions. Most of these

configurations are not calibrated for different reasons, such as large amounts of data from many seasons and many systems, unintentional time variations (failing channels), manually controlled channel gain without digital control/logging, constant upgrades during a season without the opportunity for channel equalization, lack of field calibration using active or passive targets. However, the only possible calibration for past data products is to analyze natural targets and crossovers from already existing data.

MCoRDS uses pulsed linear frequency modulation and synthetic aperture radar (SAR) processing to achieve a resolution fine enough to image ice layers. SAR data products are used in advanced processes such as tomography, basal condition estimation, roughness calculation, and realistic ice modeling [20]. Even though MCoRDS is referred to as the best of radar sounders in polar science [21], for the discovery and mapping of sub-glacial features, scientists are still being forced to use relative radiometric methods instead of absolutely calibrated data for attenuation and basal condition estimation [12], [22], [23]. Despite multiple configurations, such a system demands a proper radiometric calibration for better quality data products and inter-seasonal comparison [24].

Section II discusses this calibration problem, and presents a data-dependent calibration (based on natural targets and crossovers) for future and already existing data products. The surface and internal layers are considered specular and isotropic but the future work would address a weakly birefringent ice. Section III shows the procedure of processing data from crossover locations, a discussion of results, and a few examples of selected issues discovered through crossover analysis. Another proposed solution that uses an active target is presented in Section IV for future missions. Section V discusses concluding remarks and future work.

II. CALIBRATING AIRBORNE RADARS

A. Problems

In simple terms, radiometric calibration is the process of characterizing the radar hardware and processing parameters to produce data products that are nearly perfect estimates of a target scene. After calibration, the data products should be independent of the characterized parameters and contain only target properties, eventually facilitating a comparison of the target scene captured at a different time and/or by another radar. Accurate and precise calibration measurements are critical to mitigate errors in data products and consequently improve estimates of scientific parameters and physical models of the target.

The calibration process for a multi-channel system is a bit more complex than a single-channel system. A few of the steps are similar to the textbook SAR systems and signal processing outlined by Curlander and McDonough [25]. The system undergoes internal (radar modules are characterized and radar equation terms are measured) and external (measurements from a characterized target) calibration. After the process, it is common to specify uncertainties or error ranges for data products. Complexity often occurs during the calibration, and the

radar platform itself for airborne systems, such as MCoRDS, making difficult to calibrate using traditional methods.

MCoRDS antenna array characterization is difficult because its installation under the aircraft fuselage or wings uses materials/objects with less-known (sometimes unknown) properties and complex geometric structures. On platforms like the NASA P-3, the radar antennas use the body of an aircraft as a ground plane. Due to the lack of accurate electromagnetic models for the aircraft and MCoRDS's conformal array, errors occur due to offsets in simulated and measured array responses. In a validation flight environment (usually over water), steering vector generation is affected by the aircraft's attitude. This differs from a regular science mission with a straight heading and a level attitude over ice. Errors in steering vector estimation propagate to errors in backscatter estimation [26] and basal condition estimation.

In addition, precise internal calibration is not possible without monitoring the hardware's drift over time during a deployment season. To minimize these issues, smooth water targets with known scattering properties serve as calibration targets of opportunity that can help monitor variations in the end-to-end system. However, not every flight path crosses a natural target with known scattering properties in a regular season.

An ideal solution is to deploy an active target discussed in Section IV for precise calibration. This could solve the problems for future missions but not the past ones. The data-dependent calibration solution discussed in Section II-B is realizable and capable of calibrating current and future data products.

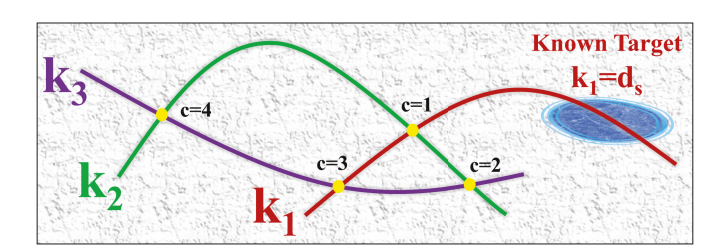


Fig. 1. Operation mode example of a Natural (known) target and Crossovers

B. Data-dependent Calibration Solution

A partial database of natural targets and crossovers is generated for a geographic section of Greenland. This will be extrapolated to include the complete set of natural targets and crossovers in the data collected by NASA Operation IceBridge (OIB). This process will check for unsaturated scattering signatures to categorize them into smooth water bodies, crossing flight paths, ground truths (such as in-situ measurements, ice cores, observation stations), etc., and location tags (such as on/off the coast, ice sheet, crevasses). A system of linear equations that links these signature terms to correction terms and calibration coefficients is formed. A simple example to explain this process is shown in Fig. 1.

To begin with, we form the specular radar equation with the receiver system gain included since this is part of what we would like to calibrate for each flight path. The equation uses reflection coefficient (Γ) and two-way spreading loss for a specular target at a distance, R, (hence $4\pi(2R)^2$) to calculate received power density. The terms in radar equation shown in (1) include the received power at the digitizer (P_r) , transmitted power (P_T) , transmitting antenna gain (G_T) , receiving antenna aperture (A_e) , and receiver system gain (G_{rx}) .

$$P_r = P_T G_T \frac{\Gamma^2}{4\pi (2R)^2} A_e G_{rx} \tag{1}$$

Rearranging the terms that remain constant for a mission and terms dependent on a known target results in (2).

$$\underbrace{k = \frac{1}{P_T G_T A_e G_{rx}}}_{\text{Calibration coefficient}} = \underbrace{\frac{\Gamma^2}{4\pi (2R)^2 P_r}}_{\text{Known target values}} \tag{2}$$

For a known target, $s \in \mathbb{N}^+$, under flight path 1:

$$k_1 = d_s \tag{3}$$

At crossovers,
$$\Gamma^2 = \underbrace{\frac{P_r 4\pi (2R)^2}{P_T G_T A_e G_{rx}}}_{\text{flight path i}} = \underbrace{\frac{P_r' 4\pi (2R')^2}{P_T' G_T' A_e' G_{rx}'}}_{\text{flight path j}} \quad (4)$$

At each crossover, $c \in \mathbb{N}^+$, for any two flight paths $(i,j) \in \mathbb{N}^+$ the above equation (4) can be rewritten by substituting in calibration coefficients (k_i,k_j) defined in (2), and defining target dependant numerators extracted from the data products, $a_c = P_r 4\pi (2R)^2, b_c = P_r' 4\pi (2R')^2$, to form:

$$\mathbf{k}_{i}a_{c} = \mathbf{k}_{i}b_{c} \tag{5}$$

$$k_i a_c - k_i b_c = 0 (6)$$

Combining (3) and (6) for the example in Fig. 1,

$$known \Rightarrow \begin{bmatrix} 1 & 0 & 0 \\ a_1 & -b_1 & 0 \\ 0 & a_2 & -b_2 \\ c = 3 \Rightarrow \\ c = 4 \Rightarrow \begin{bmatrix} a_3 & 0 & -b_3 \\ 0 & a_4 & -b_4 \end{bmatrix} \begin{bmatrix} k_1 \\ k_2 \\ k_3 \end{bmatrix} = \begin{bmatrix} d_s \\ 0 \\ 0 \\ 0 \end{bmatrix}$$

$$(7)$$

$$C \begin{bmatrix} k_1 \\ k_2 \\ k_3 \end{bmatrix} = \begin{bmatrix} d_s \\ 0 \\ 0 \\ 0 \\ 0 \end{bmatrix} \Rightarrow \begin{bmatrix} k_1 \\ k_2 \\ k_3 \end{bmatrix} = C^+ \begin{bmatrix} d_s \\ 0 \\ 0 \\ 0 \\ 0 \end{bmatrix}$$
 (8)

In a general case, the size of the Correction matrix, C, is given by $N_{rows} = (N_{KnownTargets} + N_{Crossovers})$ and $N_{columns} = N_{FlightPaths}$. Usually, $N_{columns} << N_{rows}$, hence $rank(C) = min(N_{rows}, N_{columns}) = N_{columns}$. When C has full rank, $C^+ = (C^HC)^{-1}C^H$ is the pseudoinverse. Generally, a pseudo-inverse using singular value decomposition is computed in MATLAB to avoid forcing the full rank, which results in a solution with the least norm. In either case, the resulting calibration coefficients are the optimized least squares solution and are used to calibrate

the data products. Residual analysis would provide error bars on the final results. Cases with higher residuals and other outliers will be eliminated from the natural target and crossover analysis. An absolute calibration is possible for the nadir direction and only a partial one for SAR or side-looking techniques. Ultimately, the goal of this work is to achieve the best radiometric accuracy possible. For reference, Broome and Schroeder [27] analyzed the problem of discriminating between basal targets with similar reflection coefficients. They considered radiometric accuracies of ± 0.5 dB and ± 3 dB. Although both accuracy levels could provide useful discrimination, they showed there were definite advantages to the much finer ± 0.5 dB accuracy. (Their analysis also suggests that a multi-frequency dataset is needed to fully leverage the improved radiometric accuracy.)

III. CROSSOVER ANALYSIS

A. Procedure

Crossover analysis finds reliable target signatures from crossing flight paths and pre-processes (as necessary) to coregister the waveforms pulled out from the location. Fig. 2 shows a high-level block diagram and is discussed with examples in the following sub-sections. For further information, see the OPR toolbox guide [16], [28].

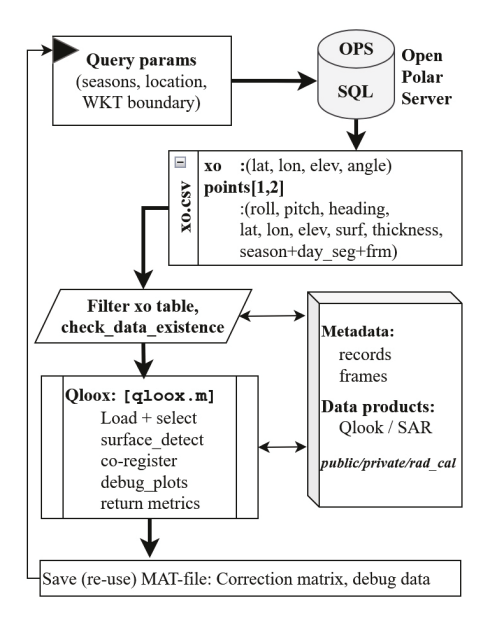


Fig. 2. Block diagram showing crossover analysis. "xo" is short for "crossover"

The crossover table is analyzed and iteratively filtered to remove outliers such as large elevation differences (>50 meters) between flight paths, rolls greater than a threshold (\pm 7 degrees, for example), and occasionally crossover angles (near-zero degrees for parallel and near 90 degrees for orthogonal analysis). This is done for both points on the flight paths so that the waveforms can have similar (backscatter) properties.

In quick-look processing for each crossover, metadata (records + frames) and data products from both flight paths are

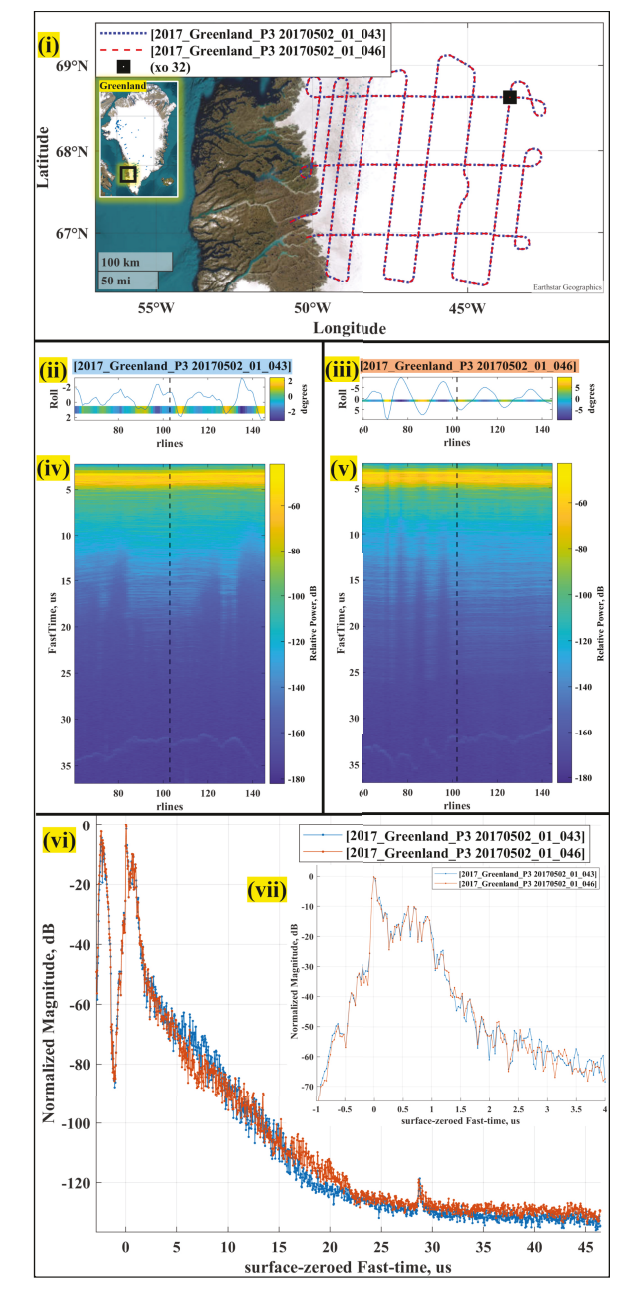


Fig. 3. Debug figures for a crossover: (i) Flight paths crossing at $\theta = 83^{\circ}$; (ii,iii) Aircraft roll; (iv,v) Partial Radiograms; (vi) Waveform comparison and (vii) Zoomed inset near surface.

loaded and truncated to select only a single range line from each flight path. For the waveforms (or the closest range lines) picked from these radargrams, the location of the surface is detected even if it is known already. The second waveform is interpolated on the fast-time axis of the first waveform and then co-registered onto the first waveform. A new fast-time axis is created with the surface at zero time to help with further analysis. The plots are usually normalized as shown in subplots (vi, vii) of Fig. 3 to see the contrast in waveform properties discussed in Section III-B or to identify issues in data products discussed Section III-C. Values such as measured power and

other metadata are returned to the calling function that saves and reuses the MAT files to continue with the calibration coefficient estimation. The entire process is repeated until each crossover in a deployment season is flagged as reliable or low quality by looking at all the basic metadata and debug figures. This ensures that extracted waveforms and data processing parameters in a season are consistent and accurate.

B. Results and Discussion

An example of a crossover from a single day segment is visualized in Fig. 3 subplot (i). Subplots (ii, iii) show the aircraft roll for the two partial radargrams shown in subplots (iv, v) that are extracted from the corresponding frames at the crossover. The vertical black dashed line indicates the range line closest to the crossover location. The effect of the aircraft roll angle on the backscatter intensity can be observed in radargrams as the internal layers fade in and out because of the varying incident angle of electromagnetic fields on the layered media. Layers are clearly visible when the aircraft roll is closer to zero and begin to disappear when the roll angle is closer to half of the array beam width (8.3 degrees for NASA P-3 center array in this example). Even though a threshold for aircraft roll is set in the crossover table, it is important to check for internal layering and adjust the threshold if necessary.

Usually, a crossover of flight paths from two different day segments helps form the equation for crossover shown in (6). However, this example shows the effect of a near-90-degree crossover angle in the same flight path at a waypoint, shown as a black square in subplot (i) just after a turn at the end of a mission line on the top right corner of the map. Subplots (vi, vii) of Fig. 3, therefore, show a mismatch in waveforms, indicating the effects of crossover angle on internal layering imaged by a single-polarized MCoRDS array.

C. Issues in Data Products

Crossover analysis helped to identify problems in the data quickly. The qloox data analyzed so far indicates that a crossover can be affected by one or more issues such as a mismatch in the processing parameters for a single or multiple waveforms, a single or multiple faulty channels, spanning a single or multiple day segments, etc.

Waveform jumps/discontinuities: MCoRDS uses multiple waveforms (usually three) with different pulse and gain settings to sound englacial targets throughout the ice column and the scattering from the basal interface underneath the ice. In the process of combining these individual images, an error in ADC gain or channel equalization magnitude causes a discontinuity in stitching the waveforms. This appears as a jump that could incorrectly indicate the presence of a bright ice layer. In a few cases, the jump completely hides the local peaks that indicate layers and the bottom.

If the raw and pulse-compressed data per channel look to be in good shape, similar to other channels, and if the only issue is an offset in signal power, then a temporary fix is to adjust channel equalization coefficients for the faulty channel to match with other channels. A better way is to look at natural

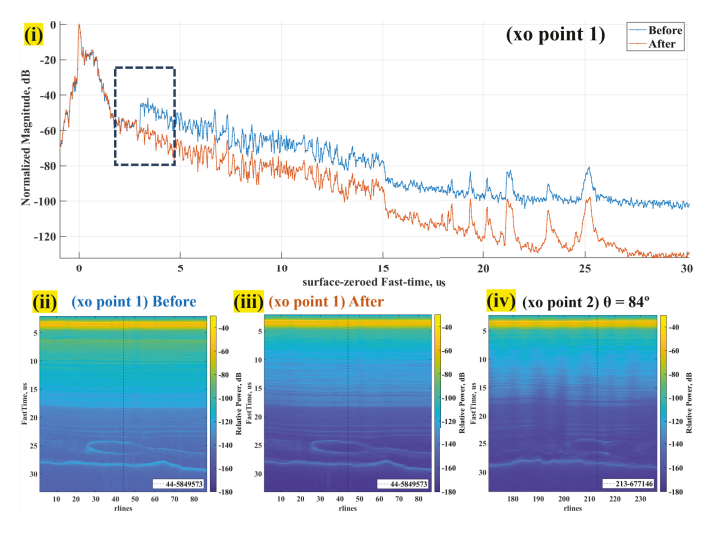


Fig. 4. Data products issues example: (i) waveforms from point 1 of a crossover before and after fixing the jump during image combining; partial radargrams from point 1 before (ii) and after (iii) fixing the jump; partial radargram from point 2 of the crossover ($\theta=84.01^{\circ}$) shown for comparison.

target responses and properly estimate channel equalization coefficients; this will be accurately fixed in future analysis of natural targets. An example of fixing jumps, shown in Fig. 4, results in accurate power levels with improved SNR for layers and bottom. Radargrams in subplots (ii, iii) show this improvement for the first point of a crossover. Radargram from the second point of the crossover in subplot (iv) shows the distortion of an elliptical 5-kilometer subglacial feature imaged at a crossover angle of 84.01 degrees.

Waveform shapes/distortions: Due to hardware issues, a few channels often produce bad waveform shapes, such as wider side lobes and distorted pulse-compressed waveforms. This issue is easily identified when the rest of the channels look good. MCoRDS samples the backscatter in the baseband through receiver modules that need frequent attention due to a moderate failure rate during the campaign. Usually termed ADC issues, these are rectified between consecutive day segments if time permits, or sometimes can go on for multiple days. By spot-checking a frame to look at individual channels and plotting normalized cross-correlation coefficients, bad channels are identified, and the parameter spreadsheets are updated to omit them from subsequent processing.

After fixing one or more of these issues in data products, a near-zero crossover angle example in Fig. 5 shows well-aligned waveforms at a crossover formed by different flight paths that are 17 days apart.

IV. PROPOSED ACTIVE TARGET SOLUTION

In the future, to avoid problems with data-dependent calibration, a simple active target with an antenna, digitally controlled waveform generator, transmitter, and receiver offers great potential to calibrate the system in a single-pass. Unlike a passive target reflector, an active target offers a higher SNR and adjustable calibration signal waveforms. During calibration mode, the airborne radar's pulse repetition interval

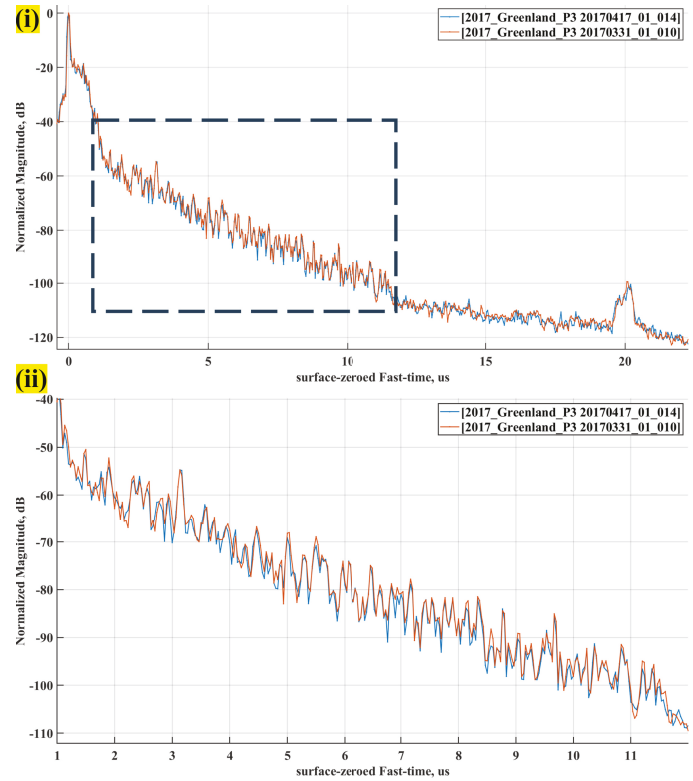


Fig. 5. An example of perfectly aligned waveforms for a near-zero crossover angle ($\theta = 0.24^{\circ}$) after fixing issues in data products. (i) crossover waveforms showing surface (0 μ s), layers, and bottom (20 μ s); (ii) zoomed plot (1 - 12 μ s) showing aligned peaks (internal layering)

could be adjusted to be longer than usual to accommodate a calibration signal from the active target, as shown in Fig. 6. The active target can also work in a smart mode where it can record the transmission in addition to broadcasting the signal back to the radar and/or transmit a recorded signal. The link budget for an active target deployed at broadside and grazing angles that can support a version of MCoRDS flying on a NASA P-3 platform is shown in Table I. If the radar's transmit signal is used for calibration, then an amplifier stage with 13 dB gain and 23 P1dB at output could be used.

V. CONCLUSION

The crossover analysis framework is complete which is used to identify and fix issues in data products. OPR toolbox scripts can now populate the crossover rows of the Correction matrix. Crossover analysis at near-orthogonal and near-zero crossover angles can provide insight into how the backscatter is affected by areas with varying ice dynamics. The next step is to build a natural target analysis framework to fill the remaining rows by identifying good natural targets for absolute calibration. This process includes a specularity analysis of data products to find smooth water under flight paths.

ACKNOWLEDGMENT

We acknowledge the use of software from Open Polar Radar generated with support from the University of Kansas,

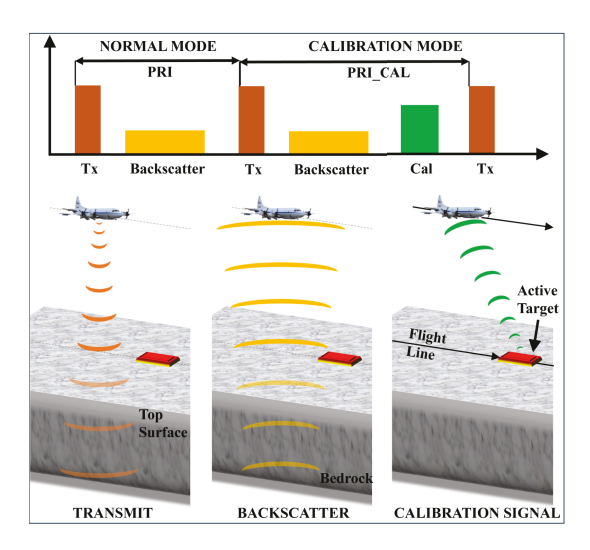


Fig. 6. Operation mode of the Active Target

TABLE I LINK BUDGET FOR THE ACTIVE TARGET

Operation parameter	Broadside (Grazing)
Radar Transmitter	
Frequency	180 – 210 MHz
Range	1500 ft
Transmit power	1000 W
Transmit antenna gain	15.45 dBi (-14.55 dBi)
Active Target Receiver	
Receive antenna gain	3 dBi (0 dBi)
Received signal power	7.00 dBm (-26.00 dBm)
Received noise power	-97.70 dBm
Received SNR	104.70 dB (71.70 dB)
Active Targ	get Transmitter
Transmit power	0.1 W
Transmit antenna gain	3 dBi (0 dBi)
Radar	Receiver
Receive antenna gain	7 dBi (-23 dBi)
Received signal power	-41.45 dBm (-74.45 dBm)
Received noise power	-95.20 dBm
Received SNR	53.75 dB (20.75 dB)

NASA grants 80NSSC20K1242 and 80NSSC21K0753, and NSF grants OPP-2027615, OPP-2019719, OPP-1739003, IIS-1838230, RISE-2126503, RISE-2127606, and RISE-2126468. We acknowledge the use of data and/or data products from CReSIS generated with support from the University of Kansas, NASA Operation IceBridge grant NNX16AH54G, NSF grants ACI-1443054, OPP-1739003, and IIS-1838230, Lilly Endowment Incorporated, and Indiana METACyt Initiative [29].

REFERENCES

- [1] IPCC, 2023: Climate Change 2023: Synthesis Report. Contribution of Working Groups I, II and III to the Sixth Assessment Report of the Intergovernmental Panel on Climate Change [Core Writing Team, H. Lee and J. Romero (eds.)]. IPCC, Geneva, Switzerland, 2023.
- [2] WCRP Global Sea Level Budget Group, "Global sea-level budget 1993present," Earth System Sci. Data, vol. 10, no. 3, pp. 1551-1590, Aug. 2018.
- [3] The NASA Global Climate Change website. [Online]. Available: https://climate.nasa.gov/

- [4] T. L. Edwards et al., "Effect of uncertainty in surface mass balance-elevation feedback on projections of the future sea level contribution of the Greenland ice sheet," *The Cryosphere*, vol. 8, no. 1, pp. 195-208, Jan. 2014.
- [5] J. L. Bamber et al., "A new bed elevation dataset for Greenland," *The Cryosphere*, vol. 7, no. 2, pp. 499-510, Mar, 2013.
- [6] J. Weertman, "Stability of the Junction of an Ice Sheet and an Ice Shelf," J. Glaciology, vol. 13, no. 67, pp. 3-11, 1974.
- [7] D. Docquier, L. Perichon and F. Pattyn, "Representing Grounding Line Dynamics in Numerical Ice Sheet Models: Recent Advances and Outlook," Surv. in Geophys., vol. 32, no. 4-5, pp. 417-435, Jun. 2011.
- [8] M. Altenburg, R. Culberg and D. M. Schroeder, "Empirical characterization of surface crevasse clutter in multi-frequency airborne ice-penetrating radar data," *IGARSS* 2022 2022 IEEE Int. Geosci. Remote Sens. Symp., Kuala Lumpur, Malaysia, 2022, pp. 1684-1687.
- [9] A. A. McLeod et al., "Processing and Detecting Artifacts in Multi-Input Multi-Output Phase-Sensitive ICE Penetrating Radar Data," IGARSS 2022 - 2022 IEEE Int. Geosci. Remote Sens. Symp., Kuala Lumpur, Malaysia, 2022, pp. 3786-3789.
- [10] T. M. Jordanet al., "Radar characterization of ice crystal orientation fabric and anisotropic viscosity within an Antarctic ice stream," J. Geophys. Res.: Earth Surf., vol 127, no. 6, Jun. 2022, Art. no. e2022JF006673.
- [11] J. T. Bessette, D. M. Schroeder, T. M. Jordan, J. A. MacGregor, "Radar-sounding characterization of the subglacial groundwater table beneath Hiawatha Glacier, Greenland," *Geophys. Res. Lett.*, vol. 48, no. 10, May 2021.
- [12] Winnie Chu et al., "Multisystem Synthesis of Radar Sounding Observations of the Amundsen Sea Sector From the 2004–2005 Field Season," J. Geophys. Res.: Earth Surf., vol. 126, no. 10, Oct. 2021.
- [13] D. M. Schroeder, "Paths forward in radioglaciology," Ann. Glaciology, vol. 63, no. 87-89, pp. 13–17, Sep. 2022.
- [14] S. D. Blunt et al., "Radar research at the University of Kansas," Proc. SPIE, Radar Sensor Technology XXI, vol. 10188, pp. 1-12, May 2017.
- [15] J. Paden et al., "Open Polar Radar Software and Services to Standardize Radar Echograms and Integrate into a Geospatial Database," presented at the AGU Fall Meeting 2021, New Orleans, LA, USA, Dec. 13-17, 2021, Paper C51A-08.
- [16] Open Polar Radar. (2023). opr (Version 3.0.1) [Computer software]. https://gitlab.com/openpolarradar/opr/ https://doi.org/10.5281/zenodo. 5683959
- [17] NSF Award 2126503. (2021). [Online]. Available: https://www.nsf.gov/awardsearch/showAward?AWD_ID=2126503
- [18] G. Raju, W. Xin, and R. K. Moore, "Design, Development, Field Observations, and Preliminary Results of the Coherent Antarctic Radar Depth Sounder (CARDS) of the University of Kansas, U.S.A.," J. Glaciology, vol. 36, no. 123, pp. 247–254, 1990.
- [19] J. A. MacGregor, L. N. Boisvert, B. Medley, A. A. Petty, J. P. Harbeck, R. E. Bell et al., "The Scientific Legacy of NASA's Operation IceBridge," *Rev. Geophys.*, vol. 59, no. 2, Jun. 2021.
- [20] J. Paden, T. Akins, D. Dunson, C. Allen and P. Gogineni, "Ice-sheet bed 3-D tomography," J. Glaciology, vol. 56, no. 195, pp. 3-11, 2010.
- [21] Joe MacGregor. (2021). [Online]. Available: https://twitter.com/ JoeMacGregor/status/1395391597429276675
- [22] J. A. MacGregor et al., "Radar attenuation and temperature within the Greenland Ice Sheet," J. Geophys. Res.: Earth Surf., vol. 120, no. 6, pp. 983–1008, Jun. 2015.
- [23] T. M. Jordan et al., "A constraint upon the basal water distribution and thermal state of the Greenland Ice Sheet from radar bed echoes," *The Cryosphere*, vol. 12, no. 9, pp. 2831-2854, Sep. 2018.
- [24] A. Freeman, "SAR Calibration: An Overview," *IEEE Trans. Geosci. Remote Sens.*, vol. 30, no. 6, pp. 1107-1121, Nov. 1992.
- [25] J. Curlander, R. McDonough, "Radiometric Calibration of SAR Data" in *Synthetic Aperture Radar: Systems and Signal Processing*. J. Kong, New York, USA: Wiley, 1991, ch. 7, pp. 310-369.
- [26] I. Ziskind, M. Wax, "Maximum Likelihood Localization of Multiple Sources by Alternating Projection," *IEEE Trans. Acoust., Speech, and Signal Process.*, vol. 36, no. 10, pp. 1553-1560, 1988.
- [27] A. L. Broome, D. M. Schroeder, "A Radiometrically Precise Multi-Frequency Ice-Penetrating Radar Architecture," *IEEE Trans. Geosci. Remote Sens.*, vol. 60, pp. 1-15, 2022, Art no. 5104515.
- [28] Open Polar Server (OPS) GeoPortal. [Online]. Available: https://ops. cresis.ku.edu/
- [29] CReSIS. 2023. MCoRDS Data, Lawrence, Kansas, USA. Digital Media. [Online]. Available: https://data.cresis.ku.edu/